GEOSPHERE

GEOSPHERE, v. 15, no. 4

https://doi.org/10.1130/GES02137.1

6 figures

CORRESPONDENCE: msawlan@usgs.gov

CITATION: Sawlan, M.G., 2019, Alteration, mass analysis, and magmatic compositions of the Sentinel Bluffs Member, Columbia River flood basalt province: REPLY: Geosphere, v. 15, no. 4, p. 1448–1458, https://doi.org/10.1130/GES02137.1.

Science Editor: Shanaka de Silva

Received 14 December 2018
Revision received 12 May 2019
Accepted 26 June 2019

Published online 2 July 2019

Alteration, mass analysis, and magmatic compositions of the Sentinel Bluffs Member, Columbia River flood basalt province: REPLY

Michael G. Sawlan

U.S. Geological Survey, 345 Middlefield Road, MS 973, Menlo Park, California 94025, USA

1. INTRODUCTION

I welcome the opportunity to continue the discussion of my mass analysis methodology, and I would like to take this opportunity to acknowledge the workers who have contributed to the extensive literature on the mapping and geochemistry of Columbia River Basalt Group (CRBG) lava flows. Notably, the junior authors of the comment by Baker et al. (2019) have produced much of the formative work on CRBG chemostratigraphy over the past several decades. To each of them I express my appreciation for providing the foundation on which I have built my own research.

In their comment, Baker et al. state that careful sampling by previous workers, and sample selection through examination of numerous thin sections, have resulted in a geochemical database for samples from the Sentinel Bluffs Member of the Grande Ronde Basalt that are mostly unaffected by secondary alteration (e.g., Reidel and Valenta, 2000). Moreover, they state that their geochemical methods are "rigorous," "well established," and have a "long history" of application in the study of CRBG lavas. They claim, however, that my mass analysis method (see Section 3) is "flawed," "invalid," and "arbitrary," and that "it seems improbable that samples with fresh outcrop appearance and commonly glassy and unaltered mineralogy in thin section could simultaneously show chemical trends resulting from considerable mineral dissolution."

In reply, I will show that *both* anoxic alteration and oxic surface weathering of CRBG lavas are prevalent both east and west of the Cascade Range, that my methodology is based on quantitative techniques that have been used in the analysis of weathered rocks and soils for decades (Nesbitt, 1979; Brimhall et al., 1992; Anderson et al., 2002), and that my own careful field and laboratory sampling, as documented in Sawlan (2018), can result in an unweathered and relatively unaltered sample collection, whereas those samples previously collected in SB lavas (e.g., Reidel and Valenta, 2000) have not only experienced significant anoxic water-rock interaction with groundwater but have subsequently undergone appreciable oxic weathering at the ground surface.

2. COMPARISON OF MASS ANALYSIS AND ROCK WEATHERING EXPRESSIONS

The mass analysis methodology introduced by Sawlan (2018) applies a fundamental term, the parent:sample immobile element ratio, which is incorporated in all prior expressions used to quantify low-temperature chemical alteration from water-rock interaction (e.g., Nesbitt, 1979; Brimhall et al., 1992; Anderson et al., 2002). This ratio equals the sample mass fraction remaining after alteration (if any), and its application as a multiplier to element abundances is termed mass-normalization (Sawlan, 2018). Baker et al. claim that these expressions are flawed and invalid, but they do not substantiate such claims. To dispel any doubt about the validity of the mass analysis methodology, here I show how these expressions relate to the expression widely applied in evaluating chemical effects of weathering.

Anderson et al. (2002) presented an expression to quantify changes in element abundances resulting from rock weathering relative to a parent rock composition in which the element-mass-transfer coefficient, tau (τ), is defined as follows,

$$\tau = \left(C_j^s \cdot C_i^p\right) / \left(C_j^p / C_i^s\right) - 1, \quad (1)$$

where the subscripts i and j refer to an immobile element and any element, respectively, and the superscript s is substituted for the subscript *w* to refer to any sample. Baker et al. (2019) refer to an expression for a "mobility ratio" (Thomson et al., 2014), but, except for a rearrangement of terms, their expression is mathematically identical to that for tau. Referring to tau as a ratio, however, is incorrect because Equation (1) shows that the expression involves four abundance terms and the subtraction of a constant.

Baker et al. contend that Equation (1) accounts for bulk density and volume changes and thereby assert that Sawlan's (2018) "data correction methodology," apparently referring to mass-normalization, is invalid because this expression does not include density and volume terms. This claim by Baker et al. is plainly incorrect: a cursory examination of Equation (1) shows that there are no terms for either volume or density.

To discuss the Equation (1) terms in a logical progression in relation to the terms used in mass analysis, Equation (1) is rearranged as follows,

$$\tau = C_i^p / C_i^s \cdot C_j^s / C_j^p - 1. \quad (2)$$

The two left terms, C_i^p / C_i^s, correspond to the parent:sample immobile element ratio, which was defined by Sawlan (2018) as the sample mass fraction (remaining), M^s, or, expressed as a percentage, the sample mass index, MI^s. Because immobile elements (IE) are not transported in low-temperature water-rock interaction, their abundances in normalized analyses (to 100% volatile-free)

of altered rock change only from depletion (or addition) of mobile elements (ME), which causes a change in sample mass. IE do not "accumulate," as described by Baker et al., but their increase in normalized abundances is simply an artifact of the analysis process whereby mass-depleted samples are analyzed as a unit mass. The multiplication of normalized element abundances by the sample mass fraction, M^s, reverses this inherent normalization and gives element abundances for a sample's mass-depleted state. As explained in Sawlan (2018), for normalized analyses of mass-altered samples IE abundances "change" as the reciprocal of the remaining sample mass fraction, $1/M^s$, and such changes are predominantly positive due to sample mass loss from mineral dissolution.

Substituting M^s for the parent:sample IE ratio, C_i^p/C_i^s, the expression for tau given in Equation (2) can be rewritten as follows,

$$\tau = M^s \cdot C_j^s / C_j^p - 1. \quad (3)$$

For IE, the product of the sample mass fraction, M^s, and sample abundances, C_j^s, removes the analytical process artifact and yields their parent abundances because these elements are conserved. For ME, this product also removes the analytical process artifact but gives their abundances as depleted (or enriched) without the normalization in proportion to depleted abundances.

Sawlan (2018) referred to the product of sample mass fraction and sample abundance, given by the two left terms of Equation (3), as "mass normalization," and the resulting value as the "mass-normalized" abundance as described by the following expression,

$$C_j^{s,mn} = M^s \cdot C_j^{s,n}, \quad (4)$$

where the superscript mn is appended to the superscript *s* to identify mass-normalized abundances, and the superscript n likewise identifies abundances from an analysis normalized to 100% volatile-free. Substituting $C_j^{s,mn}$ (Equation 4) for the equivalent terms of Equation (3) gives the following expression for tau,

$$\tau = C_j^{s,mn} / C_j^p - 1. \quad (5)$$

Equation (5) shows that tau values equal the ratio of mass-normalized to parent abundances less 1 and that the expressions of Sawlan (2018) are incorporated within this expression for tau.

The two terms in Equation (5), in addition to mass-normalized abundance, convert the mass-normalized abundance to a fraction of the parent abundance, and reference element-abundance changes to zero instead of 1. Thus, depleted and enriched ME have negative and positive tau values, respectively, and IE have a tau value of 0. Although unessential, these same two terms facilitate visual comparison of alteration-generated changes for multiple elements in relation to a unit parent abundance, such as in a vertical weathering profile. Excluding these terms allows direct examination of ME abundances (i.e., in wt% or ppm) remaining after mass changes from alteration and enables the determination of important relationships between mass-normalized abundances and remaining sample mass. These relationships will be discussed below along with the differences between alteration in reducing anoxic groundwater alteration and oxic surficial weathering, which can be used to identify the environment(s) in which the rock samples were altered.

3. PARENT COMPOSITIONS AND ALTERATION INDEXES

For mass-normalized IE abundances of Sentinel Bluffs (SB) and other CRBG lavas to correspond to parent abundances, and be applicable to making precise chemostratigraphic distinctions, parent compositions must be determined from independent criteria. Sawlan (2018) quantified SB parent IE abundances from a negative $Al_2O_3^n$-TiO_2^n magmatic trend derived from Cpx+Pl fractionation in subequal amounts. In addition, given that the dominant effect of alteration is mineral dissolution resulting in mass loss, which leads to increased IE-normalized abundances, those samples having the lowest IE abundances along the fractionation trends represent parent magmatic compositions.

Baker et al. do not acknowledge the fundamentally different influences from magmatic and alteration processes on sample chemistry, documented by Sawlan (2018), but instead evaluate Sawlan's SB samples using mafic indexes of alteration for reducing (MIA_r) and oxic conditions (MIA_o) (Babechuk et al., 2014). They assert that unaltered CRBG lavas have "typical" values for alteration indexes (MIA_r = 25–26; MIA_o = 39–40), but they do not explain how they determined that samples with these values correspond to parent compositions. They also fail to account for the differences in magmatic compositions that cause variations in parent alteration index values.

Figure 1 shows a plot of the mafic index of alteration for reducing conditions, MIA_r versus sample mass index, MI^s, for the SB analyses reported in Sawlan (2018). In this plot, samples are assigned symbols according to Sawlan's (2018) SB chemical series identified using IE ratios and mass-normalized abundances, and the physical stratigraphy. These data show a negative correlation between MIA_r and MI^s values, having a slope of approximately –0.4 over the 9 wt% range of MI^s; each unit change in MIA_r therefore is equivalent to 2.5 wt% mass loss. In their table 1, Baker et al. report MIA_r values rounded to the nearest integer, which implies that by their criteria, "unaltered" samples can be distinguished only within an uncertainty of ~2.5 wt% mass loss.

SB parent magmatic compositions are indicated for the samples in Figure 1 between the vertical dotted lines at MI^s values of 99.75 and 100.25. These sample values are used to define the MI^{100} magmatic trends (Sawlan, 2018) and span a range in MIA_r of 24.6–25.9. Differences in MIA_r values for samples from different SB series having MI^s values of ~100 correspond to differences in magmatic compositions that are not accounted for by the MIA_r alteration index. For example, SB Series V samples generally have higher MIA_r values compared to the earlier SB lavas (Series I–IV). This relative offset is maintained with decreasing MI^s values indicating that the reactive minerals were similar in composition and dissolved in similar proportions among all SB lavas (Fig. 1).

The dashed line with positive slope at MI^s ~98 in Figure 1 divides those samples with lower MI^s, identified by Baker et al. as altered, from those with higher MI^s values that they considered unaltered. The anti-correlation of MIA_r and MI^s values is maintained among samples within SB series having MI^s values of 100–97 indicating that many samples deemed "unaltered" by Baker et al. have actually lost as much as 2 wt% of their original mass from dissolution. Baker et al. interpret these samples as unaltered because of their inability to identify parent compositions in reference to magmatic processes.

A negative correlation between MI^s and MIA_r values is not surprising given that both values account for the loss of mobile elements from alteration, although in different ways. The sample mass index, MI^s, accounts for ME loss through the increase in IE abundances relative to those of unaltered magmatic compositions. The mafic indexes of alteration (Babechuk et al., 2014) are ratios of one or two IE ($Al_2O_3 \pm Fe_2O_3$) divided by the sum of the same IE and selected ME, which can be summarized by the ratio IE/IE+ME (usually expressed as a percentage). As ME are depleted by alteration, the denominator value (IE+ME) decreases relative to the numerator, and the ratio value increases. MI^s values are referenced to a magmatic value of 100% and decrease due to ME loss from alteration. On the other hand, MIA values are referenced to a value of 100 that corresponds to complete ME removal by alteration but magmatic values are undefined. Thus, with sample MIA values, there is uncertainty in parent MIA values because these are not referenced to compositions that are demonstrably magmatic in origin.

The use of MIA values is suited to characterizing relative differences in the degree of alteration for samples from an individual lava that were variably altered under the same conditions (e.g., Babechuk et al., 2014). When applied to samples whose parent magmatic compositions differ, they can give misleading results. Furthermore, MI^s values are independent of alteration conditions, but additional information is needed to determine which index (MIA_r or MIA_o) is appropriate. As will be shown, this determination can be complicated by samples that have experienced both oxic and anoxic alteration.

4. Ti-Fe VARIATIONS

Baker et al. plotted Ti-Fe variations of the Sawlan (2018) samples in which all samples were given the same symbol and noted that a negative trend expected by them between the immobile Ti and mobile Fe (for anoxic conditions) was not apparent. Figure 2 shows Ti-Fe variations for SB sample analyses given in Sawlan (2018), with samples identified by SB chemical groups. These groups include compositionally distinct lavas or possibly two flows differing only slightly in composition. The positive Ti-Fe trend at right is defined by ~70% of samples that have high MI^s values (≥99) and corresponds to a magmatic trend resulting from Cpx+Pl fractionation (Sawlan, 2018). Baker et al. postulate that Ti and Fe should be anticorrelated if the variations were due to alteration (under reducing conditions), and that Ti and Fe should be enriched and depleted, respectively. Such an inference assumes, however, a single parent

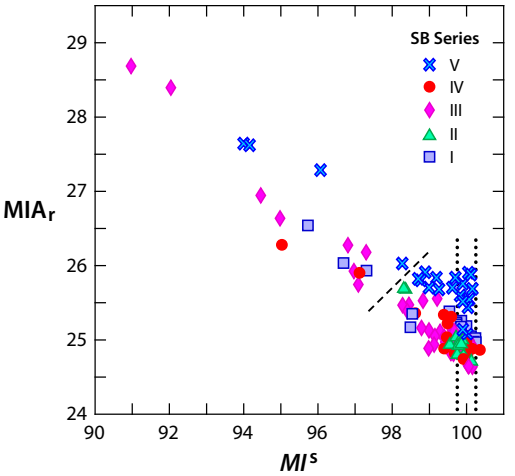

Figure 1. Mafic index of alteration for reducing conditions, MIA, (Babechuk et al., 2014), versus sample mass index, MI^s (Sawlan, 2018), for analyses of Sentinel Bluffs (SB) samples given in Sawlan (2018; supplemental file 2 therein). Data points are assigned symbols according to the SB chemical series of Sawlan (2018) as defined in the legend (upper right). Vertical dotted lines at MI^s values of 100 ± 0.25 bracket samples that define the magmatic Al-Ti "baseline" of Sawlan (2018). Dashed line divides samples considered by Baker et al. to be altered (MI^s < ~98) from those they deemed unaltered. MIA, values are dimensionless values and MI^s values are in percent of parent lava mass.

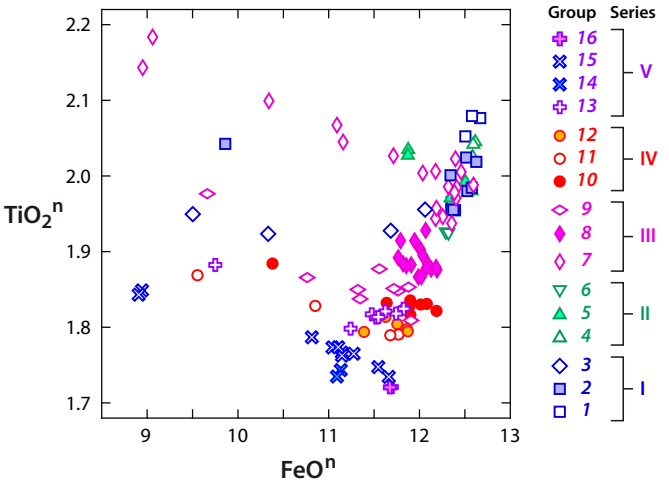

Figure 2. Variation in TiO_2^n versus FeO^n (total Fe as FeO) for Sentinel Bluffs (SB) Member samples reported by Sawlan (2018). Symbols indicate SB chemical groups as shown in legend to the right. The superscript n after the oxide symbol denotes abundances from analyses normalized to 100% volatile-free. Values are in wt%.

composition, ignores the chemostratigraphic units (SB chemical series and groups) identified by Sawlan (2018), and presumes that alteration-generated Ti-Fe variations exceed magmatic variations.

Given the large range of magmatic Ti-Fe compositions, compared to the limited range of compositional changes caused by relatively minor sample mass loss (<9 wt%), an overall negative Ti-Fe trend among all SB samples should not be expected as predicated by Baker et al. With the identification of samples by SB chemical groups in Figure 2, negative Ti-Fe trends are readily apparent among samples from individual SB groups that span a substantial range of mass loss (generally 5 wt% or more; e.g., Groups 7, 11, and 15). With the identification of magmatic compositions, the influences of alteration on lava compositions are clear. It is also apparent from the Ti-Fe relationships between parent and variably altered samples of SB groups, as well as from figure 10 of Sawlan (2018), that Fe loss is a major contributor to sample mass loss under reducing anoxic conditions.

Sawlan (2018) applied a rigorous sampling protocol that limited samples to unoxidized lava internal to alteration rinds, which yielded 70% of samples showing less than 1 wt% mass loss, with 30% of all samples showing no detectable mass loss (MI^s = 100 ± 0.25). The previously analyzed SB samples, mostly compiled by Reidel and Valenta (2000), however, exhibit a continuum in MI^s values between MI^{100} and MI^{96} (Sawlan, 2018; figure 13 therein), but there is no record of the protocol used in collecting these samples. An attempt to assess whether samples are altered or not from Al-Ti outliers in this older SB data set using an outlier identification approach would incorrectly designate samples that have lost as much as 4 wt% of their mass as unaltered.

In disregarding Sawlan's (2018) SB chemostratigraphic framework, Baker et al. present a confusing interpretation of the Ti-Fe variations shown in their figure 3. They attribute the positive Ti-Fe correlation among high-MI^s samples to "some variation in the abundance of Fe-Ti oxides in these lavas," and they speculate that I (Sawlan, 2018) would have interpreted the positive Ti-Fe trend as being caused by "leaching of Fe in these samples under reducing conditions." This, however, is incorrect in both respects. As discussed above, the positive Ti-Fe correlation does not result from Fe-Ti oxide dissolution (under reducing conditions), which instead generates negative Ti-Fe trends. The positive Ti-Fe trend among SB lavas overall is a magmatic characteristic resulting from fractional crystallization of an assemblage lacking Fe-Ti oxide, such that both Ti and Fe are concentrated in the fractionated magmas.

Moreover, Baker et al.'s interpretation that the positive Ti-Fe trend reflects differences in the abundance of Fe-Ti oxide among SB lavas implies that Fe-Ti oxide was redistributed in SB magmas prior to eruption. This interpretation is clearly incorrect. Fe-Ti oxide has been reported only as a groundmass phase in SB lavas and was not observed as a phenocryst phase in the sequential fractional crystallization (FC) experiments on tholeiitic magma having compositions similar to those of SB lavas (Villiger et al., 2007). Both Fe and Ti are concentrated in residual liquids from fractional crystallization of magma having sufficiently low oxygen fugacity to suppress Fe-Ti oxide crystallization. As discussed by Sawlan (2018), the low Fe-Mg distribution coefficient in clinopyroxene and other ferromagnesian silicates (~0.3 ± 0.03) results in Fe enrichment in the residual magmatic liquids from which such minerals have been removed by crystallization.

5. Ti-Mg VARIATIONS

Sawlan (2018; figure 12 therein) showed that low-MI^s samples from SB chemical groups have higher TiO_2^n and lower MgO^n abundances for each group than high-MI^s samples (parent abundances), and, as for the Ti-Fe variations, attributed these differences to alteration under reducing anoxic conditions. Baker et al. interpret these same sample analyses using alteration index values and a AF–CNK–M (AF–Al_2O_3 + Fe_2O_3; CNK–CaO + Na_2O + K_2O; M–MgO) ternary plot (their figure 2A). They conclude that these samples "do not display any sign of having undergone significant alteration" (except for the one oxic-weathered sample) and that they "show no evidence of Mg loss." Baker et al. therefore claim that mass-normalization (though not identified by name) consists of unjustified "arbitrary adjustments" to the analyses.

The ternary AF–CNK–M diagram shown in Baker et al.'s figure 2A is intended to illustrate the effects of oxic weathering but is inappropriate for the included SB samples of Sawlan (2018), which were altered (if at all) under anoxic conditions in which Fe (as Fe^{2+}) was mobile. With all three apexes including mobile elements, the SB samples plot in a small cluster because losses of mobile elements cancel each other and not because these samples are unaltered as claimed by Baker et al. As shown by Sawlan (2018; figure 12 therein), MgO is clearly depleted by alteration under reducing anoxic conditions.

Baker et al. subsequently present a much different interpretation based on negative tau values calculated for Fe and Mg (from unidentified parent compositions), outliers identified in the Ti-Fe sample distribution, and a trend away from the FM apex in a A–CNK–FM ternary plot, in which samples underwent Fe and Mg depletion during alteration under reducing conditions. This interpretation directly contradicts their earlier erroneous claims noted above.

6. FORENSIC CHEMICAL ASSESSMENT OF ALTERATION ENVIRONMENT AND SAMPLING PROTOCOL

Given Baker et al.'s assertion of having applied diligent sampling procedures, I have examined the SiO_2–MI^s–FeO relationships for sample data mainly from Reidel and Valenta (2000), and also from Reidel (2005) and Derkey et al. (1999, 2004). The overall data set includes analyses of samples from Basalt Waste Isolation Project (BWIP) studies, which were discussed by Landon and Long (1989) but not included in their paper.

Figure 3 presents plots of SiO_2 versus MI^s for samples from this earlier SB data set assigned to Series II–IV (Sawlan, 2018; supplemental file 1 therein), with data points color-coded by FeO abundance. MI^s values for these samples were determined using parent abundances established from a magmatic Al-Ti "baseline" (Sawlan, 2018; see figure 13 therein). This data set includes many

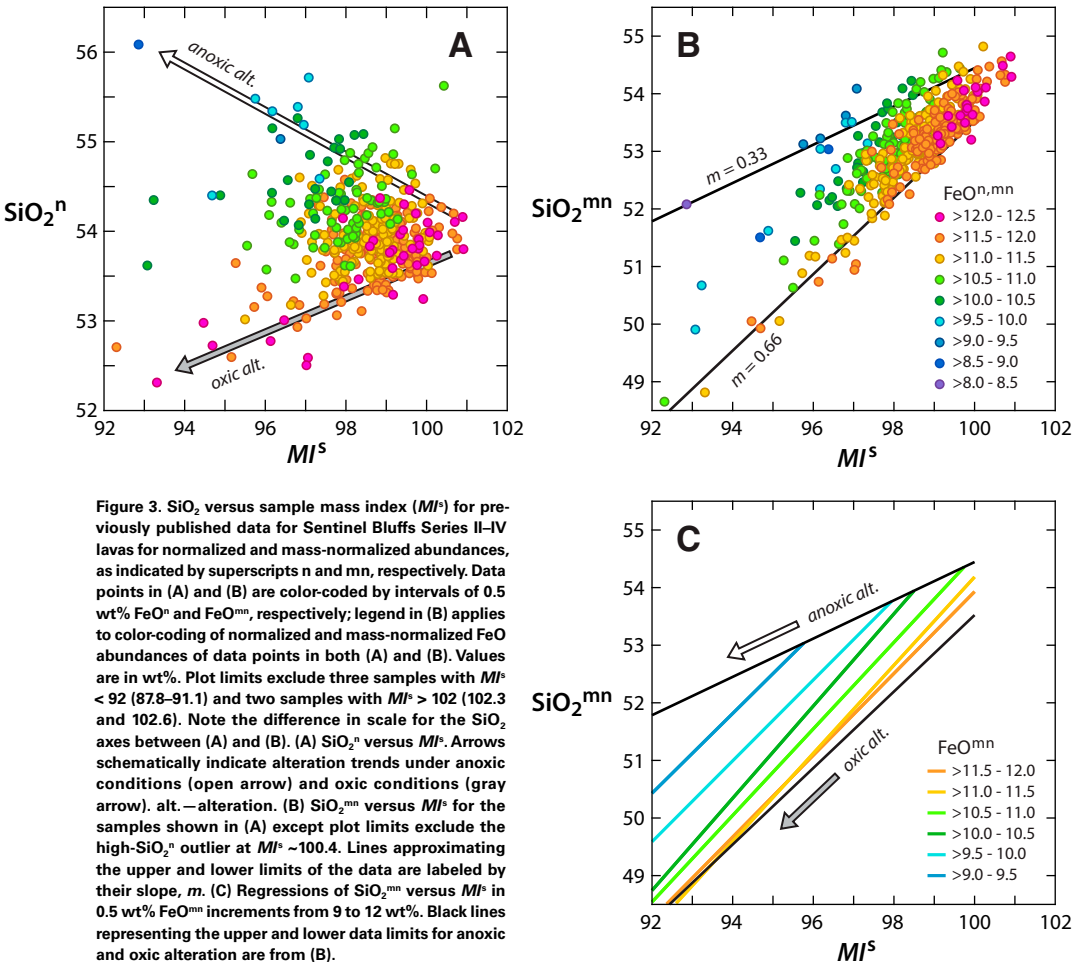

Figure 3. SiO_2 versus sample mass index (MI^s) for previously published data for Sentinel Bluffs Series II–IV lavas for normalized and mass-normalized abundances, as indicated by superscripts n and mn, respectively. Data points in (A) and (B) are color-coded by intervals of 0.5 wt% FeO^n and FeO^{mn}, respectively; legend in (B) applies to color-coding of normalized and mass-normalized FeO abundances of data points in both (A) and (B). Values are in wt%. Plot limits exclude three samples with MI^s < 92 (87.8–91.1) and two samples with MI^s > 102 (102.3 and 102.6). Note the difference in scale for the SiO_2 axes between (A) and (B). (A) SiO_2^n versus MI^s. Arrows schematically indicate alteration trends under anoxic conditions (open arrow) and oxic conditions (gray arrow). alt.—alteration. (B) SiO_2^{mn} versus MI^s for the samples shown in (A) except plot limits exclude the high-SiO_2^n outlier at MI^s ~100.4. Lines approximating the upper and lower limits of the data are labeled by their slope, *m*. (C) Regressions of SiO_2^{mn} versus MI^s in 0.5 wt% FeO^{mn} increments from 9 to 12 wt%. Black lines representing the upper and lower data limits for anoxic and oxic alteration are from (B).

samples showing alteration-generated mass loss, mostly <4 wt% (MI^s > 96), but as much as 12 wt% (MI^s ~88). Because sample mass changes from mineral dissolution could occur from either alteration under reducing anoxic conditions in groundwater or from the oxic conditions of surficial weathering, this discussion will focus first on identifying the conditions of alteration.

The plots shown in Figure 3 leverage the limited variations in parent magmatic SiO_2 and FeO abundances among SB Series II–IV lavas, as well as the large differences in alteration-generated depletions for SiO_2 and FeO between reducing anoxic and oxic conditions. Parent SB Series II–IV lavas (MI^s = 100 ± 0.25) span only 0.6 wt% SiO_2^n and 0.8 wt% FeO^n (Sawlan, 2018; supplemental file 2 therein). The limited range in magmatic SiO_2^n results from Cpx+Pl fractionation in subequal amounts, which generates only minor Si enrichment and only slightly greater Fe enrichment (Villiger et al., 2007).

Figure 3A shows normalized SiO_2 abundances (SiO_2^n) from the older SB data set as a function of sample mass index (MI^s), with samples color-coded by FeO^n abundance. Overall, these samples define a distinctive pattern, a fanning array from a narrow range in SiO_2^n at MI^s ~100 to both higher and lower SiO_2^n with decreasing MI^s, such that SiO_2^n abundances span nearly 4 wt% at MI^s ~93. FeO^n abundances decrease sharply with decreasing MI^s and increasing SiO_2^n along the upper bound of this array. FeO^n abundances, however, remain near

parent FeO^n abundances and SiO_2^n decreases with decreasing MI^s along the lower bound of this array.

To understand the origin of this sample distribution, variations in normalized and mass-normalized SiO_2 and FeO abundances as a function of MI^s are examined for samples from individual lavas altered exclusively under either reducing anoxic or oxic conditions. Samples from the higher-Ti SB Group 7 lava, which were altered (if at all) under anoxic conditions, are plotted in Figures 4A and 4C. Samples from a basalt of Dodge member lava, Wanapum Basalt (herein, "Dodge") (Thomson et al., 2014), which were altered under oxic weathering conditions, are plotted in Figures 4B and 4D. The Dodge parent composition differs from that of SB compositions in having ~2 wt% lower SiO_2 and FeO (with total Fe as FeO) and may not be precisely applicable to SB compositions; however, the Dodge samples illustrate the fundamental differences in chemical changes resulting from oxic alteration as compared to anoxic alteration.

Figure 4A shows that normalized SiO_2 abundances (open symbols) for the mass-depleted higher-TiO_2 SB Group 7 samples (altered under anoxic conditions) increase with decreasing sample mass. This increase in SiO_2^n abundances from mineral dissolution under anoxic conditions may seem counterintuitive, but the increase is an artifact of the analysis process which imparts an inherent normalization of analyses for mass-depleted rock to 100% in proportion to depleted abundances. When the aggregate SiO_2 abundance of the dissolved minerals is less than that of the parent (MI^{100}) abundance, the SiO_2 depletion from alteration is exceeded by the increase from the inherent normalization discussed earlier, resulting in an increase in normalized abundances. In Figure 4B, which shows the Dodge samples altered under oxic conditions, SiO_2^n decreases slightly with decreasing MI^s, which indicates that the SiO_2 abundance of the dissolved minerals exceeds that of the parent.

The mass-normalized SiO_2 abundances, SiO_2^{mn}, shown in Figure 4A (solid symbols), clearly show that SiO_2 is depleted, not enriched, relative to the parent abundance for alteration under anoxic conditions. The mass-normalized SiO_2 abundances for the oxic-weathered Dodge samples (Fig. 4B, solid symbols),

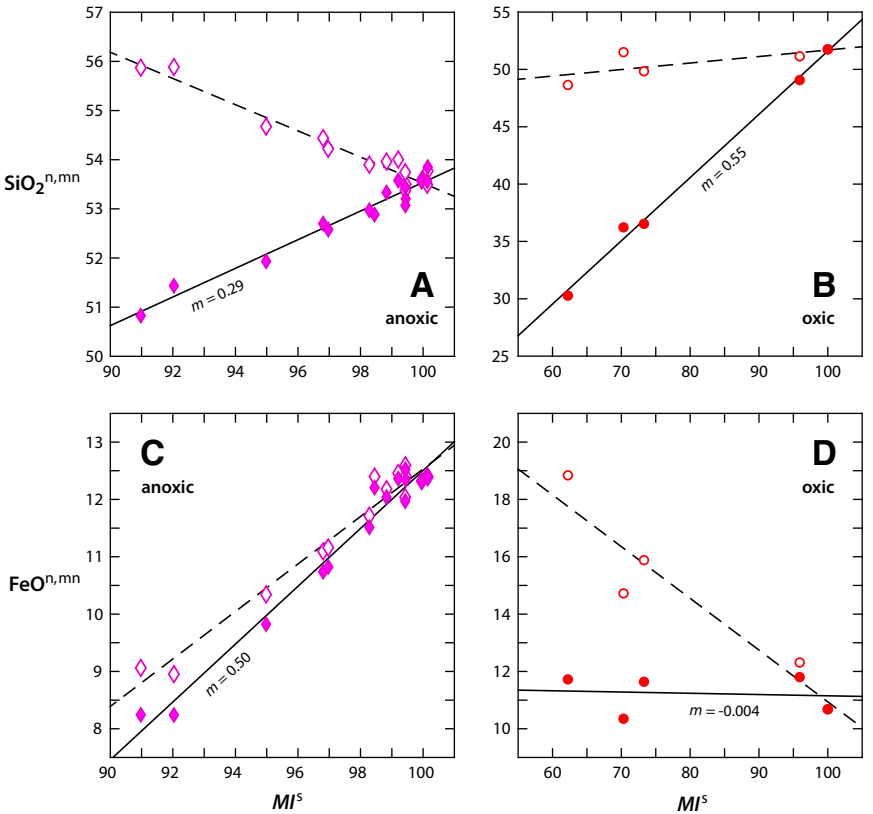

Figure 4. Plots comparing SiO_2 and FeO normalized abundances (open symbols) and mass-normalized abundances (solid symbols) as a function of sample mass index, MI^s, for alteration under reducing anoxic conditions (A and C) and under oxic conditions (B and D). Values are in wt%; FeO values are with all Fe as FeO. Sample data shown in (A and C) are for the higher-Ti Sentinel Bluffs (SB) Group 7 samples (Sawlan, 2018), and those shown in (B and D) are for the basalt of Dodge samples reported by Thomson et al. (2014). Note that for samples having MI^s values near 100, the symbols for normalized sample abundances nearly coincide with those for mass-normalized abundances. Regressions for normalized and mass-normalized abundances are shown with dashed and solid lines, respectively, and the slope, *m*, is indicated for the regressions of mass-normalized abundances. MI^s values for the SB samples were determined using TiO_2^n abundances with a parent TiO_2^n value established by a magmatic Al-Ti trend (Sawlan, 2018); MI^s values for the basalt of Dodge samples were determined from TiO_2^n abundances by adopting the sample having the lowest TiO_2^n as the parent.

however, show that SiO_2 is more strongly depleted under oxic conditions than under anoxic conditions.

For both anoxic and oxic alteration, the changes in SiO_2^n and SiO_2^{mn} with MI^s are linear, which indicates that steady-state mineral (±glass) dissolution is the predominant influence on the chemistry of altered, mass-depleted samples. The slope of the variation of mass-normalized abundances of any element as a function of MI^s gives the fraction of the total mass removed by mineral dissolution. For instance, a slope of 1 would indicate that the element accounts for all mass loss, and a slope of zero would indicate that the element accounts for none of the mass loss (i.e., for an immobile element). As such, SiO_2 accounts for 29 wt% of the material transported under anoxic conditions but accounts for nearly double this amount, 55 wt%, under oxic conditions (Figs. 4A and 4B). The linear ME depletions with MI^s in both environments not only enable the identification of those ME that have been depleted but enable the weight percentage of the total material removed to be quantified.

Figures 4C and 4D show equivalent variations for FeO^n and FeO^{mn} with MI^s for the same samples as in Figures 4A and 4B, respectively, and illustrate the difference in Fe mobility between anoxic and oxic alteration. FeO^n is strongly depleted with decreasing MI^s in the reducing anoxic environment (Fig. 4C, open symbols), and the slope of FeO^{mn}–MI^s variations, 0.50, indicates that FeO accounts for half of the total mass loss (Fig. 4C, solid symbols). For oxic alteration, FeO^n increases with decreasing MI^s (Fig. 4D, open symbols), but the approximately zero slope of FeO^{mn}–MI^s variations (Fig. 4D, solid symbols) shows that Fe effectively behaved as an IE.

Baker et al. generally attributed Fe and Mg depletion in the SB samples of Sawlan (2018) to ferromagnesian mineral dissolution. The high proportion of FeO of the total mass loss for anoxic alteration, ~50 wt%, far exceeds that of any silicate in SB lavas and clearly indicates that the Fe depletion results primarily from Fe-Ti oxide alteration in which Fe is transported and Ti is retained. While Baker et al. emphasize thin-section examination to identify samples lacking alteration, the alteration of opaque oxides would only be apparent with the examination of polished sections using reflected-light microscopy.

These differences in Si and Fe behavior between the anoxic and oxic alteration environments relate to differences in phase reactivity in these two environments, and, for Fe, differences in the solubility of Fe^{2+} and Fe^{3+}. The difference in Fe solubility exerts a major influence on the composition of the material transported from mineral dissolution, and, because this difference results from an integral difference in its oxidation state, there is not a continuum of element depletion amounts between anoxic and oxic alteration.

Returning to the SiO_2-MI^s-FeO variations for the earlier SB data set (Fig. 3), the divergent SiO_2^n limiting trends of the fanning array shown in Figure 3A are readily explained by alteration exclusively under either reducing anoxic or oxic conditions. This explains the paired decrease in FeO^n and increase in SiO_2^n with decreasing sample mass, MI^s, along the anoxic alteration trend (e.g., Figs. 4A and 4C), and the persistence of high FeO^n and the decrease in SiO_2^n with decreasing MI^s along the oxic alteration trend (e.g., Figs. 4B and 4D). The mass-normalized SiO_2^n abundances, SiO_2^{mn}, demonstrate, however, that SiO_2 is depleted in both alteration environments but at a much higher rate under oxic conditions (Fig. 3B).

Most samples from the older SB data set plot between the limiting trends of anoxic and oxic alteration (Figs. 3A and 3B), however, and their analyses cannot be explained by alteration solely under either condition. The FeO^{mn} abundances of such samples (Fig. 3B) provide clear insights into their alteration history. The samples plotting between the limiting trends form bands of samples having subequal FeO^{mn} abundances subparallel to the oxic alteration trend indicating that these samples were "weathered" under oxic conditions under which Fe is immobile. This is more explicitly illustrated in Figure 3C, which shows regressions of sample FeO^{mn} in 0.5 wt% intervals, the same intervals used to color-code the data points in Figure 3B. For samples with $FeO^{mn} < 11$ wt%, the regressions intersect the anoxic limiting trend at progressively lower MI^s values. This indicates that samples between the limiting trends require a two-stage alteration process in which the samples were initially altered under reducing anoxic conditions and subsequently altered under oxic conditions.

7. GLASS REACTIVITY IN ANOXIC AND OXIC ALTERATION ENVIRONMENTS

Baker et al. also emphasize that the presence of "fresh, unaltered" glass in samples, as identified from petrographic examination, indicates a lack of chemical alteration. In addition, they suggest it is "improbable" that "commonly glassy" samples could show chemical trends resulting from mineral dissolution.

Figure 5 compares the variations in K_2O^{mn} abundances as a function of remaining sample mass (MI^s) for samples altered under reducing anoxic conditions (in groundwater) (Fig. 5A) and under the oxic conditions of surficial weathering (Fig. 5B). Samples plotted in Figure 5A are the higher-TiO_2 SB Group 7 samples, and those plotted in Figure 5B are the Dodge samples (Thomson et al., 2014) identified earlier. The SB samples altered under reducing anoxic conditions generally have higher K_2O^{mn} abundances than high-MI^s samples, which indicate non-systematic K enrichment on the order of several tenths of a weight percent compared to high-MI^s samples. This shows that glass reactivity under reducing conditions is minimal, such that it is not dissolved to any appreciable extent. It is also consistent with the low depletion of SiO_2, which comprises only ~29 wt% of the material transported for anoxic alteration (Fig. 4A), whereas glass compositions in SB lavas are dacitic to marginally rhyolitic (~65%–73%) (Hoover and Murphy, 1989).

In contrast to the K enrichment shown for reducing anoxic conditions, the K_2O^{mn} abundances for the Dodge samples are strongly depleted with decreasing MI^s (Fig. 5B), which, given that the K is concentrated in groundmass glass during lava solidification, clearly indicates glass dissolution during oxic surficial weathering. Glass dissolution in this environment is also consistent with higher SiO_2 depletion associated with oxic weathering, which, as shown earlier, is about twice the rate for alteration under anoxic conditions.

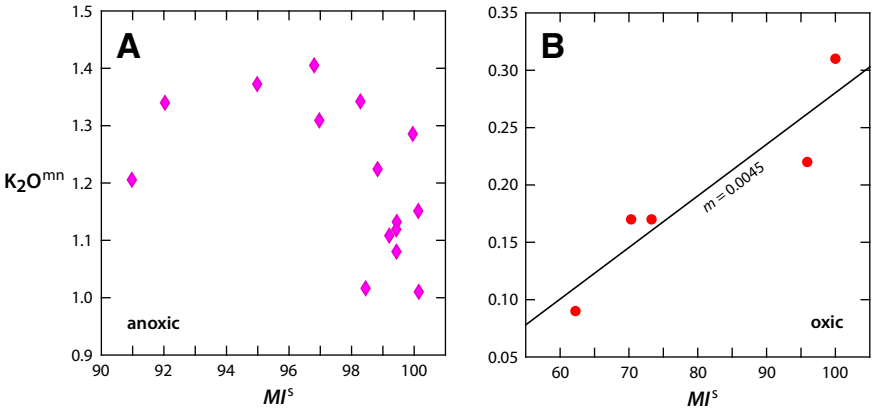

Figure 5. Mass-normalized K_2O abundances (K_2O^{mn}) versus sample mass index (MI^s) comparing samples altered under reducing anoxic and oxic conditions. Values are in wt%. (A) Higher-Ti Sentinel Bluffs Group 7 samples (Sawlan, 2018) as in Figures 4A and 4C altered (if at all) under reducing anoxic conditions. (B) Basalt of Dodge samples reported by Thomson et al. (2014) as in Figures 4B and 4D altered under the oxic conditions of surficial weathering. The slope, *m*, is given for the regression line shown in (B).

The K_2O^{mn}-MI^s variations (Fig. 5A), together with the SiO_2^{mn}-MI^s variations (Fig. 4A) show that glass is minimally reactive and is not dissolved to an appreciable extent under reducing anoxic conditions. The use of petrographic identification of "fresh" glass, therefore, is not a diagnostic criterion for establishing whether or not a sample has undergone chemical alteration. Samples altered under oxic weathering conditions, however, undoubtedly show evidence of glass dissolution and, likely, partial replacement by secondary minerals. Such samples can be readily identified in hand specimen from the obvious visual cues (color, texture, and secondary minerals) associated with oxic surficial weathering. Furthermore, Baker et al. cite only 766 thin sections of SB samples compared to 2268 SB samples analyzed. This disparity indicates that thin-section examination was not consistently applied in evaluating SB samples for chemical analysis.

8. INTRAFLOW CHEMICAL VARIATIONS AND LAVA FLOW MIXING

In their figure 1, Baker et al. present a vertical profile showing TiO_2 and P_2O_5 abundances for samples from a borehole in the Pasco Basin; this figure was presented first in Reidel (2005) and has been presented in multiple papers since. Despite having ample opportunity to present the underlying data and appropriate documentation (e.g., stratigraphic position, accurate location coordinates, analysis date, sampling protocol, sample context, and sampling geologist), Reidel (±coauthors), and now Baker et al., still have not presented the analyses and documentation that would allow independent evaluation of these data.

Sawlan (2018) showed that 16 compositionally distinct SB groups within five chemical series can be distinguished by IE ratios and abundances of samples that have retained their original mass, or nearly so. Moreover, mass-depleted samples can be related to specific chemical groups from their mass-normalized IE abundances as well as to the broader SB series from their IE ratios. Following Reidel's (2005) lead, Baker et al. base their interpretations of lava flow chemical heterogeneity entirely on variations in the normalized abundances of Ti and P, both of which can be modified by alteration. Furthermore, they hypothesize that four separately and simultaneously erupted lavas flowed long distances and eventually comingled and mixed in the Pasco Basin area, by "multiple-flow injection" according to Reidel (2005). They claim that this process resulted in flow intervals or "layers" (Reidel, 2005) distinguished by their Ti and P abundances, within the SB Group 11 flow (Sawlan, 2018), which was informally named the Cohassett flow during the BWIP studies. Notably, Baker et al. do not present an alteration assessment of the analyses used in their figure 1 as was done for the Sawlan (2018) SB samples.

Baker et al.'s figure 1 shows that high Ti and P abundances in samples from the Cohassett flow's top and bottom are confined within the flow contacts. Other profiles given in figure 6 of Reidel (2005) (RRL-6, White Salmon), however, show that his "compositional types" traverse flow boundaries. This indicates that such compositional differences are postemplacement chemical characteristics that may occur from preferential alteration of the more porous flow tops and bottoms of successively emplaced flows.

Furthermore, Baker et al.'s claim that four compositionally distinct lava flows erupted simultaneously is not supported by the physical stratigraphy. They infer that the high-Mg lavas assigned to their Airway Heights and California Creek compositional types, which are found only in the northeastern Columbia Basin, erupted at the same time as the SB lavas assigned to the Stember Creek and Spokane Falls types. The Airway Heights and California Creek lavas, however, could be significantly older than SB lavas because their lower possible stratigraphic position is poorly constrained. Other high-Mg lavas (Slack Canyon and Indian Ridge GRB members) having limited extents within the Columbia Basin are known to have erupted during the GRB N_2 magnetozone prior to SB eruptions (Landon and Long, 1989; Reidel et al., 1989; Reidel and Tolan, 2013).

In addition, neither the Airway Heights nor California Creek lavas are found in a stratigraphic succession with the SB Group 11 (Stember Creek) lava. The intraflow chemical differences therefore are more plausibly explained by differential alteration of the dense and porous parts of the lava flows.

9. GEOGRAPHIC DISTRIBUTION OF ANOXIC GROUNDWATER ALTERATION AND OXIC SURFICIAL WEATHERING

From the common occurrence of thick paleosols formed by surficial weathering west of the Cascade Range, Baker et al. contend that CRBG lavas in the Columbia Basin to the east of the Cascades have remained unaffected by any alteration. The type of alteration identified by Sawlan (2018), however, is not visually apparent and is caused by interaction with anoxic groundwater. Alteration under anoxic conditions can occur anywhere within the flood basalt province given that these lavas currently host aquifers on both sides of the Cascades and have undoubtedly done so for the past ~16 m.y. Baker et al.'s claim of no anoxic alteration east of the Cascades also contradicts statements elsewhere in their comment, in which they discuss "early" leaching of Mg and Fe under reducing conditions from altered CRBG lava in southeastern Washington and nearby Idaho (e.g., Thomson et al., 2014).

The assertion by Baker et al. that CRBG lavas east of the Cascades in the Columbia Basin are mostly unaffected by surficial weathering, even in recent road cuts, is simply not true. Figure 6 shows examples of alteration rinds and weathered rock in road cuts and natural exposures in various parts of the Columbia Basin (northeastern, southeastern, south-central, and southwestern) not scoured by the Missoula floods (Sawlan, 2018). Areas where the floods were erosive tend to have thin alteration rinds from the removal of weathered rock, but such areas are not representative of the flood basalt province as a whole. Thick concentric weathering rinds are commonly encountered in the Columbia Basin and can be up to ~15 cm thick in some outcrops. In some instances, oxic surficial weathering is pervasive, or nearly so, such that many fracture-bounded blocks lack a "corestone" of less altered or possibly unaltered inter-rind rock. In each Columbia Basin location where small corestones were sampled from within thicker weathering rinds, multiple fracture-bounded blocks that were broken open contained only weathered rock.

10. CONCLUSIONS

The mass analysis expressions used to determine the remaining sample mass and mass-normalized abundances (Sawlan, 2018) are incorporated within those expressions that have been widely used in rock and soil weathering studies (e.g., Anderson et al., 2002). They differ from those applied in conventional weathering studies, however, in two important respects: (1) mass-normalized abundances are not converted to a dimensionless ratio of the parent abundance from which a value of 1 is subtracted, but are presented directly in wt% or ppm. This allows direct comparison of mass-normalized abundances for altered and unaltered samples; and (2) parent abundances are referenced to a magmatic trend between immobile elements (Al and Ti), thereby establishing a unit parent mass to which altered samples are referenced. Parent compositions of altered samples can be determined from their Al/Ti ratios, and, as in conventional expressions, the parent:sample ratio of an immobile element (e.g., Ti) is used to quantify the remaining sample mass. It appears that Baker et al. did not compare the simple expressions for sample mass index and mass-normalization to the terms in the expression for tau given by Anderson et al. (2002). As shown above, the mass analysis (Sawlan, 2018) and weathering (Anderson et al., 2002) calculations are in complete agreement. Therefore, if the mass analysis formulas are incorrect, then those given in Nesbitt (1979), Brimhall et al. (1992), and Anderson et al. (2002), as well as Baker's own "mobility ratio" (Thomson et al., 2014), are also incorrect.

Baker et al. state that "good" samples can be obtained with care in "collection and preparation," and that "excellent samples" can be obtained "if one takes care and collects unaltered rock from the core of altered columns." Workers with decades of experience are said to have established a "standard procedure" to avoid sampling altered rock, but descriptions of such a procedure cannot be found in the methods sections of prior reports. Baker et al. cite Swanson and Wright (1981) as an example of the standard sampling procedure for CRBG lavas, but Swanson and Wright did not discuss their sampling protocol.

Baker et al. also claim that identification of (apparently) unaltered glass using petrographic examination is sufficient to characterize a sample as unaltered. This criterion does not apply, however, to samples altered under anoxic reducing conditions due to the low reactivity of glass relative to that of Fe-Ti oxide and pyroxene. Although glass is altered in surficially weathered samples, thin-section examination is not necessary to identify oxic weathering because there are other visual cues indicating this type of alteration. Furthermore, excluding one strongly oxic-weathered sample intentionally collected, all SB samples collected by Sawlan (2018), without benefit of thin-section examination, showed no detectable chemical evidence of oxic alteration. In addition, 70% of Sawlan's (2018) analyses indicated less than 1% mass loss, and, among the samples exhibiting mass loss, progressive Fe depletion with decreasing sample mass showed they were altered exclusively under reducing anoxic conditions.

Despite the general agreement of Baker et al. with Sawlan (2018) that alteration of a subset of samples reported in Sawlan (2018) occurred under reducing conditions, there are important differences stemming from the different approaches. Baker et al. cannot identify specific parent compositions of lavas such that they can only broadly characterize the chemical effects of alteration. As shown in Sawlan (2018), together with the analysis given in this reply, the application of mass analysis can (1) quantify alteration in terms of a physical property, (2) identify parent compositions, (3) quantify a threshold of alteration, and (4) determine the composition of the material removed by dissolution.

Sawlan (2018) showed that the earlier SB data set includes many samples showing mass loss, mainly <4%, as well as some samples showing higher

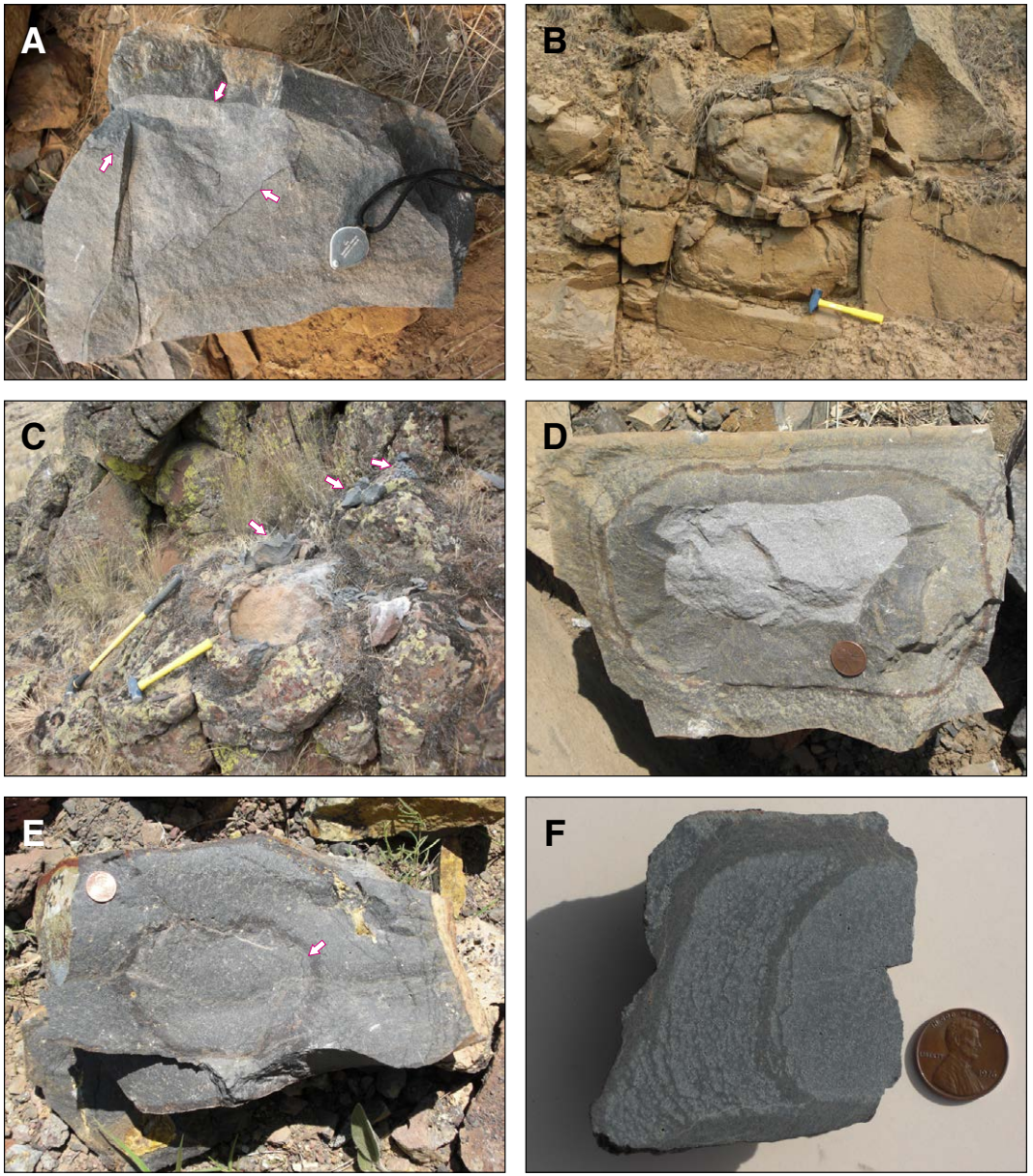

Figure 6. Photographs of Grande Ronde Basalt lava flows within the Columbia Basin showing weathering characteristics relevant to sampling. (A) Sample of the informally named California Creek flow in the northeastern Columbia River Basalt province, at the California Creek section, located ~25 mi SSE of Spokane, Washington. Two generations of alteration rind enclose a lighter-colored corestone. The lower two arrows indicate a thin dense rind along the contact between oxidized rock and corestone. The upper arrow indicates the contact between corestone and a dense, dark-gray rind, which crosscuts both corestone and oxidized rind. Lupe for scale has long dimension of 2.5 cm. (B) Road-cut exposure of the Sentinel Bluffs (SB) flow likely corresponding to Sawlan's (2018) SB Group 10, which overlies the flow in (A). Inward progression of alteration has left corestones enclosed by thick alteration rinds. (C) Sample site in the upper part of a Grande Ronde Basalt section located along the north side of the Snake River, 2 km WNW of Steptoe Canyon and ~13 km northwest of Clarkston, in southeastern Washington. Thick weathering rind has a greenish-yellow lichen-encrusted surface that is removed in center of photo. From lower left to upper right, arrows sequentially indicate blocks extracted from the corestone, hand-sample–sized specimens partially cleaned of alteration, and rock chips (~2 cm across) cleaned by further sampling. The flow is a R_2 Grande Ronde Basalt, likely within the Wapshilla Ridge Member. (D) Light-colored corestone within concentric alteration rinds in the basalt of Stember Creek (as mapped by Hooper and Gillespie, 1996), southeastern Washington. Sample is from a road-cut exposure along the Alpowa Grade (U.S. Route 12), ~25 km west of Clarkston, Washington. Coin for scale is 1.9 cm across. (E) Sample of a Sentinel Bluffs Group 15 flow in Butler Canyon, southwestern Columbia Basin. Sample site is in a road cut along U.S. Route 197 ~6 km north of the town of Tygh Valley, Oregon. Photo shows a cross-sectional view of part of a column in columnar-jointed lava from ~1 m above a pillowed flow base. The gray corestone is within a thin, dark-colored rind (arrow) that is enclosed by a gray alteration rind. Nearby analyzed samples indicate 6% mass loss from alteration (see Sawlan, 2018; supplemental file 2, analyses for "SB_Sec_Flow" BL-6). Coin in upper left is 1.9 cm across. (F) Polished slab cut from a Winter Water Member flow exposed in a road cut along State Route 206 next to Wallace Canyon, ~13 km ENE of Condon, Oregon, south-central Columbia Basin. The complex alteration rind includes two dark, dense bands, separated by thin anastomosing rindlets, with a small gray corestone next to the coin (1.9 cm diameter).

amounts of mass loss, up to 12%. Most of these samples experienced alteration under oxic surficial weathering conditions, such that these samples undoubtedly exhibited characteristic color changes associated with Fe oxidation. Although Baker et al. claim they exercised diligence in applying a sampling protocol similar to that described in Sawlan (2018), supplemented by petrographic examinations, the chemical evidence indicates otherwise.

A complete data set of the earlier SB analyses, accompanied by the appropriate documentation to allow independent evaluation of these data, must be published. Following Reidel (2005), Baker et al. have interpreted sample analyses from the earlier SB database to represent magmatic compositions, but most of these samples were variably altered under both anoxic and oxic conditions. Intra-flow chemical differences, therefore, are most likely due to alteration of chemically homogeneous lava flows fed by well-mixed magma reservoirs rather than to "comingling and mixing" at the surface of four presumably coeval and compositionally distinct lava flows. In addition, previously proposed SB chemostratigraphies are inexact because magmatic compositions could not be distinguished from those modified by alteration.

ACKNOWLEDGMENTS

Constructive reviews of the manuscript by Jon Hagstrum significantly improved the manuscript and are much appreciated. Shan de Silva is to be commended for his editorial handling as well as for his review comments.

REFERENCES CITED

Anderson, S.P., Dietrich, W.E., and Brimhall, G.H., Jr., 2002, Weathering profiles, mass-balance analysis, and rates of solute loss: Linkages between weathering and erosion in a small, steep catchment: Geological Society of America Bulletin, v. 114, p. 1143–1158, https://doi.org/10.1130/0016-7606(2002)114<1143:WPMBAA>2.0.CO;2.

Babechuk, M.G., Widdowson, M., and Kamber, B.S., 2014, Quantifying chemical weathering intensity and trace element release from two contrasting basalt profiles, Deccan Traps, India: Chemical Geology, v. 363, p. 56–75, https://doi.org/10.1016/j.chemgeo.2013.10.027.

Baker, L.L., Camp, V.E., Reidel, S.P., Martin, B.S., Ross, M.E., and Tolan, T.L., 2019, Alteration, mass analysis, and magmatic compositions of the Sentinel Bluffs Member, Columbia River flood basalt province: COMMENT: Geosphere, v. 15, https://doi.org/10.1130/GES02047.1.

Brimhall, G.H., Chadwick, O.A., Lewis, C.J., Compston, W., Williams, I.S., Danti, K.J., Dietrich, W.E., Power, M.E., Hendricks, D., and Bratt, J., 1992, Deformational mass transport and invasive processes in soil evolution: Science, v. 255, p. 695–702, https://doi.org/10.1126/science.255.5045.695.

Derkey, R.E., Hamilton, M.M., and Stradling, D.F., 1999, Preliminary geologic maps of the Spokane NE and SE 7.5-minute quadrangles, Spokane County, Washington: Olympia, Washington Division of Geology and Earth Sciences Open File Report 99-6, Washington Department of Natural Resources.

Derkey, R.E., Hamilton, M.M., and Stradling, D.F., 2004, Geologic map of the Airway Heights 7.5-minute quadrangle, Spokane County, Washington: Olympia, Washington Division of Geology and Earth Sciences Open File Report 2004-1, Washington Department of Natural Resources.

Hooper, P.R., and Gillespie, B.A., 1996, Geologic map of the Pomeroy area, southeastern Washington: Olympia, Washington Division of Geology and Earth Resources Open File Report 96-5, 1 sheet, scale 1:24,000, pamphlet 26 p., Washington Department of Natural Resources.

Hoover, J.D., and Murphy, W.M., 1989, Quench fractionation in Columbia River basalt and implications for basalt-ground water interaction, *in* Reidel, S.P., and Hooper, P.R., eds., Volcanism and Tectonism in the Columbia River Flood-Basalt Province: Geological Society of America Special Paper 239, p. 307–320, https://doi.org/10.1130/SPE239-p307.

Landon, R.D., and Long, P.E., 1989, Detailed stratigraphy of the N_2 Grande Ronde Basalt, Columbia River Basalt Group, in the central Columbia Plateau, *in* Reidel, S.P., and Hooper, P.R., eds., Volcanism and tectonism in the Columbia River Flood Basalt Province: Geological Society of America Special Paper 239, p. 55–66, https://doi.org/10.1130/SPE239-p55.

Nesbitt, H.W., 1979, Mobility and weathering of rare earth elements during weathering of a granodiorite: Nature, v. 279, p. 206–210, https://doi.org/10.1038/279206a0.

Reidel, S.P., 2005, A lava flow without a source: The Cohassett flow and its compositional components, Sentinel Bluffs Member, Columbia River Basalt Group: The Journal of Geology, v. 113, p. 1–21, https://doi.org/10.1086/425966.

Reidel, S.P., and Tolan, T.L., 2013, The Grande Ronde Basalt, Columbia River Basalt Group, *in* Reidel, S.P., Camp, V.E., Ross, M.E., Wolff, J.A., Martin, B.S., Tolan, T.L., and Wells, R.E., eds., The Columbia River Flood Basalt Province: Geological Society of America Special Paper 497, p. 117–153, https://doi.org/10.1130/2013.2497(05).

Reidel, S.P., and Valenta, M.M., 2000, Preliminary chemistry, petrology, and paleomagnetism data for the Sentinel Bluffs Member, Columbia River Basalt Group: Richland, Battelle Pacific Northwest Laboratories Report PNWD-3063, 279 p.

Reidel, S.P., Tolan, T.L., Hooper, P.R., Beeson, M.H., Fecht, K.R., Bentley, R.D., and Anderson, J.L., 1989, The Grande Ronde Basalt, Columbia River Basalt Group; Stratigraphic descriptions and correlations in Washington, Oregon, and Idaho, *in* Reidel, S.P., and Hooper, P.R., eds., Volcanism and Tectonism in the Columbia River Flood Basalt Province: Geological Society of America Special Paper 239, p. 21–53, https://doi.org/10.1130/SPE239-p21.

Sawlan, M.G., 2018, Alteration, mass analysis, and magmatic compositions of the Sentinel Bluffs Member, Columbia River flood basalt province: Geosphere, v. 14, p. 286–303, https://doi.org/10.1130/GES01188.1.

Swanson, D.A., and Wright, T.L., 1981, The regional approach to studying the Columbia River Basalt Group, *in* Subbarro, K.V., and Sukheswala, R.N., eds., Deccan Volcanism and Related Basalt Provinces in Other Parts of the World: Geological Society of India Memoir 3, p. 58–80.

Thomson, B.J., Hurowitz, J.A., Baker, L.L., Bridges, N.T., Lennon, A.M., Paulsen, G., and Zacny, K., 2014, The effects of weathering on the strength and chemistry of Columbia River basalts and their implications for Mars Exploration Rover Rock Abrasion Tool (RAT) results: Earth and Planetary Science Letters, v. 400, p. 130–144, https://doi.org/10.1016/j.epsl.2014.05.012.

Villiger, S., Ulmer, P., and Muntener, O., 2007, Equilibrium and fractional crystallization experiments at 0.7 GPa; the effect of pressure on phase relations and liquid compositions of tholeiitic magmas: Journal of Petrology, v. 48, no. 1, p. 159–184, https://doi.org/10.1093/petrology/egl058.